Acta Crystallographica Section D
Biological Crystallography
ISSN 0907-4449

Structures and molecular-dynamics studies of three active-site mutants of bovine pancreatic phospholipase A_2

Shankar Prasad Kanaujia and Kanagaraj Sekar*

Bioinformatics Centre (Centre of Excellence in Structural Biology and Biocomputing), Supercomputer Education and Research Centre, Indian Institute of Science, Bangalore 560 012, India

Correspondence e-mail: sekar@physics.iisc.ernet.in, sekar@serc.iisc.ernet.in

Received 27 June 2008
Accepted 19 July 2008

PDB References: bovine pancreatic phospholipase A_2, H48N, 2zp4, r2zp4sf; D49N, 2zp3, r2zp4sf; D49K, 2zp5, r2zp4sf.

Phospholipase A_2 hydrolyzes phospholipids at the *sn*-2 position to cleave the fatty-acid ester bond of L-glycero-phospholipids. The catalytic dyad (Asp99 and His48) along with a nucleophilic water molecule is responsible for enzyme hydrolysis. Furthermore, the residue Asp49 in the calcium-binding loop is essential for controlling the binding of the calcium ion and the catalytic action of phospholipase A_2. To elucidate the structural role of His48 and Asp49, the crystal structures of three active-site single mutants H48N, D49N and D49K have been determined at 1.9 Å resolution. Although the catalytically important calcium ion is present in the H48N mutant, the crystal structure shows that proton transfer is not possible from the catalytic water to the mutated residue. In the case of the Asp49 mutants, no calcium ion was found in the active site. However, the tertiary structures of the three active-site mutants are similar to that of the trigonal recombinant enzyme. Molecular-dynamics simulation studies provide a good explanation for the crystallographic results.

1. Introduction

Phospholipase A_2 (PLA_2; EC 3.1.1.4) is an enzyme that specifically hydrolyzes the *sn*-2 fatty-acid acyl bond of phospholipids, producing a free fatty acid and a lyso-phospholipid in a calcium-dependent reaction (van Deenen & de Haas, 1964). It is involved in a number of physiologically important cellular processes such as the liberation of arachidonic acid from membrane phospholipids (van den Berg *et al.*, 1995). In addition, it plays a pivotal role in the biosynthesis of prostaglandin and other mediators. Thus, the enzyme PLA_2 is of great pharmaceutical concern since it is responsible for the release of arachidonic acid, the subsequent conversion of which produces leukotrienes and prostaglandins, which are part of the inflammatory response. The enzyme PLA_2 is widely distributed in snakes, lizards, bees and mammals. Irrespective of origin, the primary structures of most PLA_2s show a high degree of homology (Verheij *et al.*, 1981). Bovine pancreatic PLA_2 belongs to the IB group of the PLA_2 family and consists of 123 amino-acid residues with a molecular weight of ~14 kDa. It contains five α-helices, two β-strands and seven disulfide bonds, which keep the enzyme very stable, even at high temperature (Dijkstra *et al.*, 1978).

The catalytic network of the secretory PLA_2s is characterized by a catalytic dyad (Asp99–His48), a water molecule (which acts as a nucleophile during the enzymatic reaction), a calcium-binding loop and possibly other factors that stabilize the transition state (Fig. 1). In addition, the catalytic dyad residues play an important structural role (Li & Tsai, 1993).

Methylation of His48 $N^{\delta1}$ showed that the $N^{\delta1}$ atom acts as the proton acceptor during catalysis and a total loss of enzymatic activity was observed even though the binding of the substrate and the functionally important calcium ion remained intact (Verheij *et al.*, 1980). Solution studies on the single mutant H48Q suggested that His48 $N^{\epsilon2}$ was mimicked by the amide N atom of a glutamine residue and that His48 $N^{\delta1}$ can be mimicked by the amide N atom of an asparagine residue in the H48N mutant (Leatherbarrow & Fersht, 1987; Li & Tsai, 1993). Biochemical studies on the single mutant H48N showed a low (6×10^{-5}) catalytic activity compared with the wild-type enzyme (Li & Tsai, 1993). Thus, it is of interest to study the crystal structure of the single mutant H48N.

The functionally important calcium ion is liganded by three backbone O atoms from Tyr28, Gly30 and Gly32, both carboxylate O atoms of Asp49 and two water molecules (Dijkstra *et al.*, 1981; Sekar, 2007). With some exceptions, the calcium-binding pocket is also conserved. The residue Asp49 has been shown to be very important since its carboxylate O atoms are found to provide coordination of the calcium ion (van den Bergh *et al.*, 1988; Li *et al.*, 1994; Davidson & Dennis, 1990). Li and coworkers used site-directed mutagenesis and NMR studies to provide insight into the structural and functional roles of the highly conserved residue Asp49 and observed that the mutants D49N and D49K do not bind the calcium ion. However, the mutant D49E binds the calcium with 12-fold weaker binding affinity and the specific catalytic activities of these mutant enzymes decrease significantly (ranging from 5.4×10^2-fold to 5.8×10^2-fold in comparison with that of the wild-type enzyme; Li *et al.*, 1994; Sekar *et al.*, 1999). Furthermore, structural analysis using two-dimensional proton NMR indicated no global perturbation in the single mutants D49N and D49K. Thus, the aim of the proposed work was to solve the three-dimensional crystal structures of the active-site mutants H48N, D49N and D49K in order to gain a better understanding of the nature of the structural perturbations caused by Asp49 mutants and to study the effect of asparagine at position 48. In addition, molecular-dynamics (MD) simulations of the active-site mutants and three *in silico* generated mutants (1mkt_H48N, 1mkt_D49N and 1mkt_D49K) were carried out to observe the effect of these mutants on calcium binding.

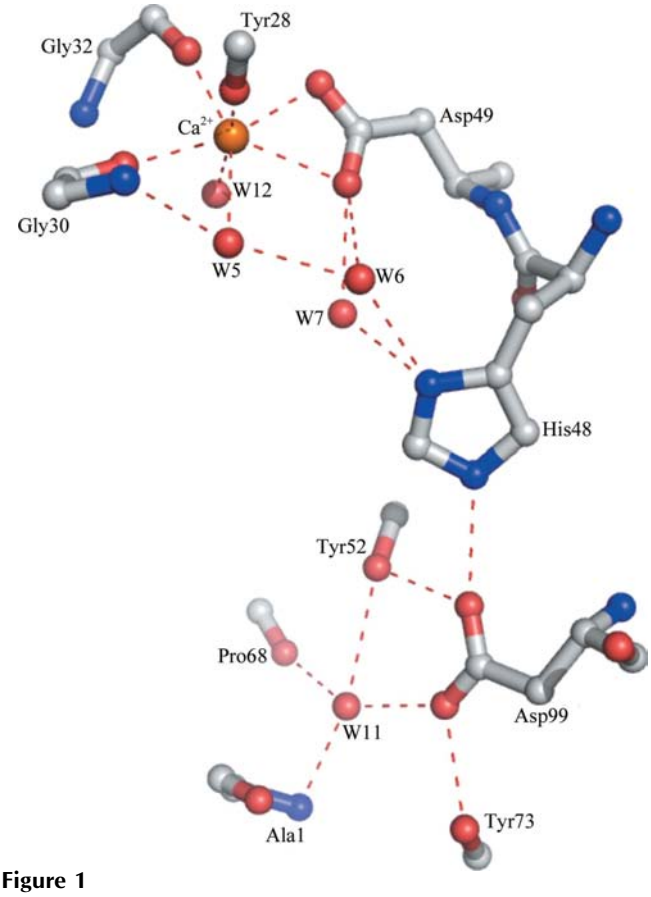

Figure 1
Active-site hydrogen-bonding network of the trigonal form of bovine pancreatic phospholipase A_2. The PDB entry used in the calculation is 1mkt.

2. Materials and methods

2.1. Purification and crystallization

Professor M.-D. Tsai of the Chemistry Department, Ohio State University supplied the three active-site mutants reported here. The procedures for the purification of these mutants were similar to those described elsewhere (Noel *et al.*, 1991; Dupureur, Yu, Jain *et al.*, 1992; Dupureur, Yu, Mamone *et al.*, 1992; Li & Tsai, 1993). The proteins were concentrated to ~15 mg ml^{-1} in 50 m*M* Tris–HCl buffer pH 7.2 and 5.0 m*M* $CaCl_2$. Crystals of all three mutants were obtained using the hanging-drop vapour-diffusion method at room temperature (293 K). In the case of the H48N mutant, the droplet consisted of 5 µl protein solution and 2 µl 50%(*v*/*v*) 2-methyl-2,4-pentanediol (MPD) and was equilibrated against 60%(*v*/*v*) MPD in 0.5 ml reservoir solution. In the case of the D49N mutant, the droplet contained 5 µl protein solution and 1 µl 60%(*v*/*v*) MPD. In the case of the D49K mutant, the droplet contained 5 µl protein solution and 3 µl 60%(*v*/*v*) MPD. In the cases of both D49N and D49K, the droplets were equilibrated against 70%(*v*/*v*) MPD.

2.2. Data collection and processing

The intensity data for all three mutants were collected at 100 K using a MAR 345 imaging-plate detector mounted on a Rigaku RU-300 generator (operated at 40 kV and 80 mA) using the home source available at the Molecular Biophysics Unit, Indian Institute of Science, Bangalore, India. The data were processed and scaled using *DENZO* and *SCALEPACK* from the *HKL* suite (Otwinowski & Minor, 1997). The intensities were converted to structure factors using the *TRUNCATE* program from the *CCP*4 suite (Collaborative Computational Project, Number 4, 1994). Crystal data and data-collection statistics are given in Table 1.

2.3. Structure refinement, validation and analysis

The crystals were isomorphous to the trigonal form of the recombinant enzyme with space group $P3_121$ and unit-cell

Table 1
X-ray data-collection and refinement statistics for three active-site mutants of bovine pancreatic phospholipase A_2.

Values in parentheses are for the highest resolution shell.

	H48N	D49N	D49K
Space group	$P3_121$	$P3_121$	$P3_121$
Unit-cell parameters (Å)	a = 45.82, c = 101.50	a = 45.79, c = 101.94	a = 46.19, c = 101.92
Crystal dimensions (mm)	0.8 × 0.3 × 0.3	0.6 × 0.5 × 0.4	0.6 × 0.3 × 0.2
Resolution range (Å)	30.0–1.9	30.0–1.9	30.0–1.9
Observed reflections	116803	116580	69065
Unique reflections	10227 (970)	9760 (918)	10359 (1011)
Completeness (%)	99.7 (99.5)	94.8 (93.7)	98.8 (99.6)
R_{merge}† (%)	5.8 (41.8)	5.4 (14.6)	5.3 (30.8)
R_{work} (%)	17.8	19.1	19.7
R_{free} (%)	20.1	23.8	23.5
Protein model			
Protein atoms	955	957	958
Water molecules	132	139	127
Metal ions	2 Ca^{2+}, 1 Cl^-	1 Ca^{2+}, 1 Cl^-	1 Ca^{2+}, 1 Cl^-
MPD	1	1	—
Tris	—	1	—
Deviations from ideal geometry			
Bond lengths (Å)	0.004	0.006	0.004
Bond angles (°)	1.2	1.3	1.3
Dihedral angles (°)	21.8	22.3	22.8
Improper angles (°)	0.69	0.79	0.79
Average temperature factors (Å^2)			
Main-chain atoms	27.01	20.10	30.65
Side-chain atoms	30.02	23.14	33.74
Water molecules	39.78	36.70	42.56
Metal ions	27.17	21.25	36.05
Ramachandran plot			
Most favoured (%)	92.7	92.7	90.9
Additionally allowed (%)	7.3	7.3	9.1
Estimated coordinate error (Å)	0.18	0.19	0.20

† $R_{merge} = \sum_{hkl}\sum_i |I_i(hkl) - \langle I(hkl)\rangle| / \sum_{hkl}\sum_i I_i(hkl)$, where $I(hkl)$ is the intensity of reflection hkl, $\sum_{hkl}$ is the sum over all reflections and $\sum_i$ is the sum over i measurements of reflection hkl.

parameters $a = b = 46.78$, $c = 102.89$ Å (PDB code 1mkt; Sekar *et al.*, 1998). Even though the crystals are isomorphous to the native structure, the three-dimensional structures of the three mutants were solved using the molecular-replacement program *Phaser* (Read, 2001; McCoy *et al.*, 2007). The three-dimensional atomic coordinates of the trigonal form of the wild type (1mkt) were used as the search model for the molecular-replacement calculations. The log likelihood gain and Z scores for H48N, D49N and D49K were 1188.35 and 41.44, 978.67 and 33.21, and 1170.18 and 34.89, respectively.

2.3.1. Refinement of H48N. The molecular-replacement solution was used as the initial model without the mutated residue Asn48. A total of 10% (1073) of the reflections were set aside for R_{free} calculations (Brünger, 1992). After a total of 50 cycles of rigid-body refinement followed by 50 cycles of positional refinement using *CNS* (Brünger *et al.*, 1998), R_{work} and R_{free} were 30% and 31%, respectively, for 8976 reflections in the resolution range 30.0–1.9 Å. Subsequently, the mutated residue Asn48 was modelled and fitted using difference electron-density maps and the model was subjected to simulated annealing by heating the system to 3000 K and slowly cooling to 100 K in 10 K steps. Strong electron density was observed for the functionally important active-site calcium ion and a chloride ion and these were added to the refined model. At this stage, R_{work} and R_{free} dropped to 24% and 28%, respectively. A large electron density (7σ) near the C-terminus was observed which was identified as a calcium ion as found previously (Sekar *et al.*, 2006). Water molecules were located and added using difference electron-density maps with peak heights greater than 2.8σ and at hydrogen-bonding distances of 3.6 Å or less to protein atoms or other water molecules. The final refined model contains 955 protein atoms, two calcium ions, one chloride ion, 132 water O atoms and one MPD molecule.

Although correct assignments of the atoms of the amide group (side-chain atoms $O^{\delta1}$ and $N^{\delta2}$) of asparagine are considered to be difficult, the widely accepted hydrogen-bonding environment schemes were followed. Furthermore, positional and B-factor refinements were carried out for both orientations of the amide group and that with the lower average temperature factor (19.84 Å^2 compared with 20.13 Å^2) was considered in further analysis. Subsequently, this was verified using the programs *MolProbity* (Davis *et al.*, 2004) and *HBPLUS* (McDonald & Thornton, 1994), which suggested the correct orientation (W6 hydrogen bonded to Asn48 $O^{\delta1}$ and Asp99 $O^{\delta1}$ hydrogen bonded to Asn48 $N^{\delta2}$) to be that identified above, in contrast to previous studies (Li & Tsai, 1993).

2.3.2. Refinement of D49N and D49K. A similar approach was followed to refine the other two mutant (D49N and D49K) structures. After initial refinement of the model, it was observed that there was no electron density for the functionally important calcium ion in the active site. As observed in the H48N mutant, there was a strong electron density near the C-terminus of the Asp49-mutant structures (12σ for D49N and 7σ for D49K). In both of the Asp49 mutants a chloride ion was found near Lys12.

In summary, for all three mutants the program *CNS* (Brünger *et al.*, 1998) was used for the refinement. The molecular-modelling program *Coot* (Emsley & Cowtan, 2004) was used to display the electron-density maps for model fitting and adjustments. All atoms were refined with unit occupancies. Simulated-annealing OMIT maps were calculated using *CNS* and used to correct or to check the final protein models using the modelling program *Coot*. The simulated-annealed OMIT maps calculated at the end of the refinement were also used to check the final protein models. The program *PROCHECK* (Laskowski *et al.*, 1993) was used to validate and to check the quality of the final refined models. Figures were generated using the program *PyMOL* (DeLano Scientific

LLC; http://www.pymol.org). The web-based programs *PDB Goodies* (Hussain *et al.*, 2002) and 3*dSS* (Sumathi *et al.*, 2006) were used for the analysis and superposition. The details of the refinement of all three mutants are given in Table 1.

2.4. Molecular-dynamics simulation

Energy minimization and simulations were performed using *GROMACS* v.3.3 (van der Spoel *et al.*, 2005) with the OPLS-AA/L all-atom force field (Jorgensen *et al.*, 1996; Kaminski *et al.*, 2001). Energy minimization was performed using the conjugate-gradient method for 200 ps with the maximum force field cutoff being 1 kJ mol^{-1}. The recombinant wild-type PLA_2 structure (PDB code 1mkt) was mutated *in silico* using the program *Coot* at positions 48 (for H48N) and 49 (for D49N and D49K) with the corresponding residues and these structures are abbreviated as 1mkt_H48N, 1mkt_D49N and 1mkt_D49K, respectively. However, the functionally important calcium ion was retained in all three *in silico* mutants in order to observe the effect of the mutation on the calcium during molecular dynamics. The *in silico* mutants were checked for stereochemistry. The crystallographic water molecules were removed and protein models were solvated with the SPC (simple point charge) water model using the *genbox* program available in the *GROMACS* suite. The box size of the system was 6.4 × 6.4 × 6.4 nm. Sodium and chloride ions were used to neutralize the overall charge of the system. Simulations utilized NPT ensembles with isotropic pressure coupling (τ_p = 0.5 ps) to 1 bar and temperature coupling (τ_t = 0.1 ps) to 300 K. Parrinello–Rahman and Nose–Hoover coupling protocols were used for pressure and temperature, respectively. Long-range electrostatics were computed using the Particle Mesh Ewald (PME) method (Darden & York, 1993) and Lennard–Jones energies were cut off at 1.0 nm. Bond lengths were constrained with the *LINCS* (Hess *et al.*, 1997) algorithm. The parameters and topology files for MPD and Tris molecules were generated using the *PRODRG* server (Schüttelkopf & van Aalten, 2004). Analyses were primarily performed with tools available in the *GROMACS* suite. The average structures used for comparison and analysis were calculated using ensembles generated between 2 and 3 ns. The ensembles were computed every 2 ps.

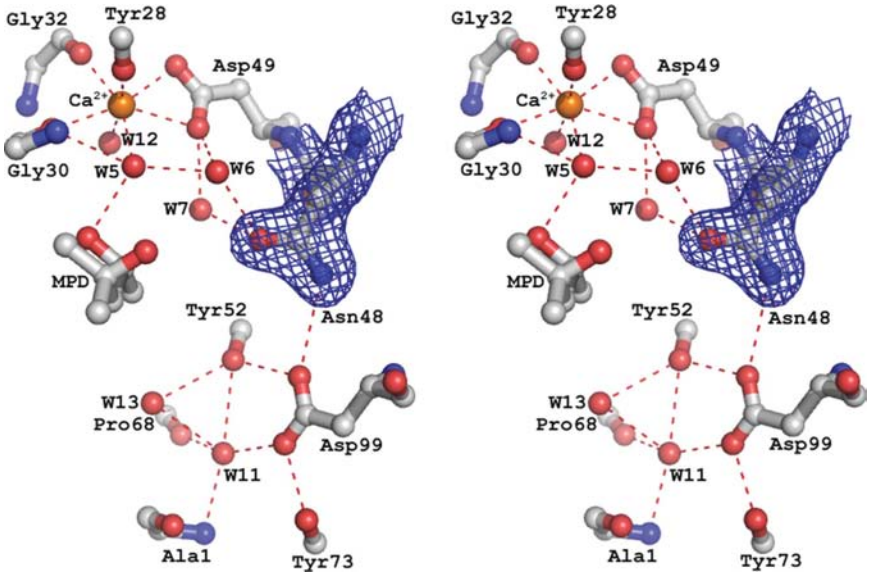

Figure 2
Active-site hydrogen-bonding network of the H48N mutant. The $2|F_o| - |F_c|$ electron-density map for the mutated residue asparagine is contoured at 1.0σ.

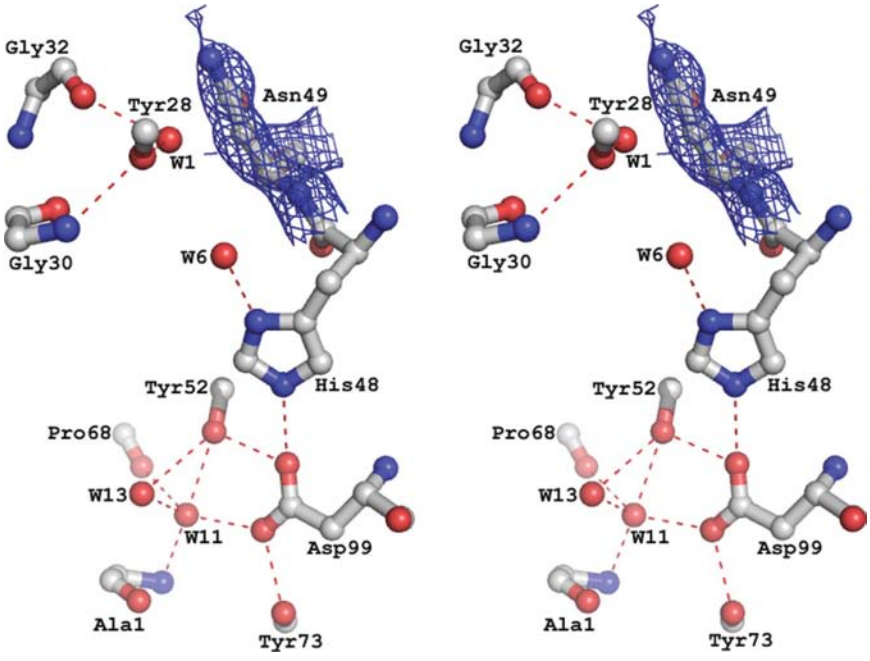

Figure 3
Active-site hydrogen-bonding network of the D49N mutant. The $2|F_o| - |F_c|$ electron-density map of Asn49 is shown at 1.0σ.

3. Results and discussion

3.1. H48N mutant

Previous NMR studies on the H48N mutant suggested that the mutation at His48 affects the overall tertiary structure (Li & Tsai, 1993). In contrast to the NMR studies, the tertiary structure is intact in the crystal structure of H48N and is highly similar to that of the trigonal wild-type PLA_2 (PDB code 1mkt), with a root-mean-square deviation (r.m.s.d.) of 0.3 Å (for the backbone atoms). The five protein ligands of the active-site calcium ion superpose with an r.m.s.d. of 0.15 Å with the trigonal wild type.

The calcium–ligand distances vary between 2.26 and 2.60 Å, with an average of 2.46 Å, which is slightly higher than the average of 2.39 Å obtained from the atomic resolution structure (Steiner *et al.*, 2001). This is probably a result of the lower resolution of the present structure. An MPD molecule is observed in the vicinity of the active site and is hydrogen bonded to the equatorial water molecule (W5) as found previously (PDB code 1vl9; Sekar *et al.*, 2005). A water molecule (W13) is hydrogen bonded (Fig. 2) to the structural water (W11). This water molecule is observed in the orthorhombic wild-type PLA_2 (PDB code 1une) and the single mutants H48Q (PDB code 1kvw) and D49N (PDB code 2zp3). A previous study of the single mutant H48Q (Sekar *et al.*, 1999) revealed that Gln48 $N^{\varepsilon 2}$ is hydrogen bonded to Asp99 $O^{\delta 1}$ and Gln48 $O^{\varepsilon 1}$ is hydrogen bonded to the catalytic water molecule (W6). However, in the single mutant H48N both catalytic water molecules (W6 and W7) are hydrogen bonded to Asn48 $O^{\delta 1}$.

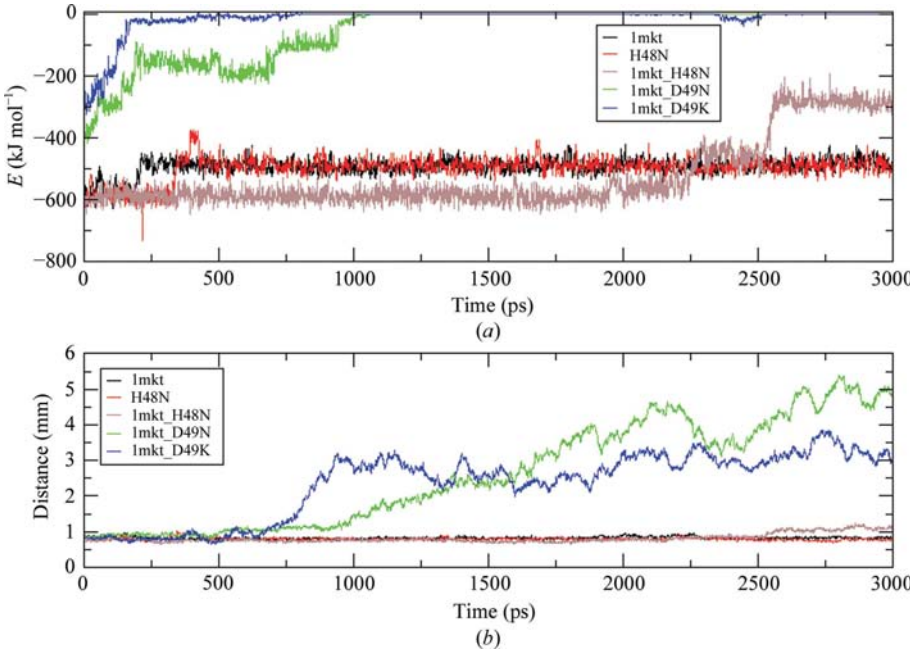

Figure 4
The graphs shows (*a*) protein–calcium ion interaction energy and (*b*) protein–calcium ion distance during the molecular-dynamics simulation of 3 ns. The graph was generated using the program *GRACE* (http://plasma-gate.weizmann.ac.il/Grace/).

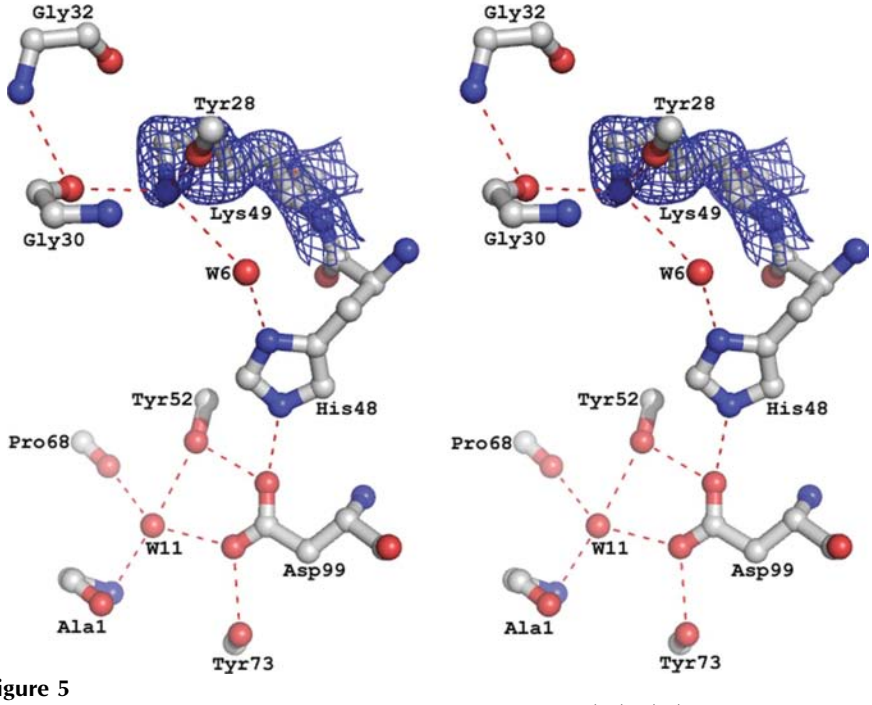

Figure 5
Active-site hydrogen-bonding network of the D49K mutant. The $2|F_o| - |F_c|$ electron density of the mutated residue lysine is shown at 1.0σ. Only two active-site water molecules (W6 and W11) are observed of the five commonly found water molecules. The distance between $N^{\xi}(49)$ and the catalytic water W6 is 3.34 Å.

Interestingly, the hydrogen bonding between Asn48 $N^{\delta 2}$ and Asp99 $O^{\delta 1}$ is retained in the structure. However, unlike His48, the mutant Asn48 cannot act as a base to accept a proton from the catalytic water (W6). Surprisingly, however, solution studies showed a low (6×10^{-5}) residual catalytic activity in the H48N mutant compared with the wild-type enzyme (Li & Tsai, 1993). It is widely accepted that His48 is involved in the activation of the catalytic water (W6) to initiate the reaction. However, the possibility exists that a similar role could be fulfilled by Asp49, which is on the other side (Fig. 1) of the catalytic water (W6$\cdots$Asp49 $O^{\delta 1}$ = 2.9 Å). The very low catalytic activity in the present mutant H48N is presumably the consequence of the acceptance of a proton by the residue Asp49 from the catalytic water W6.

Molecular-dynamics simulations were performed after solvating the crystal structure of the H48N mutant for a time period of 3 ns. Careful examination of the average structure shows that five water molecules provide coordination of the calcium ion. Two of the water molecules occupy the positions of the two important axial (W12) and equatorial (W5) coordination water molecules generally found in the crystal structure of PLA_2. Interestingly, after MD simulation, three water molecules are found at the positions of W7, W11 and W13, as in the crystal structure. In order to verify the chosen orientation of the amide group of the mutated residue Asn48 ($O^{\delta 1}$ hydrogen bonded to W6,

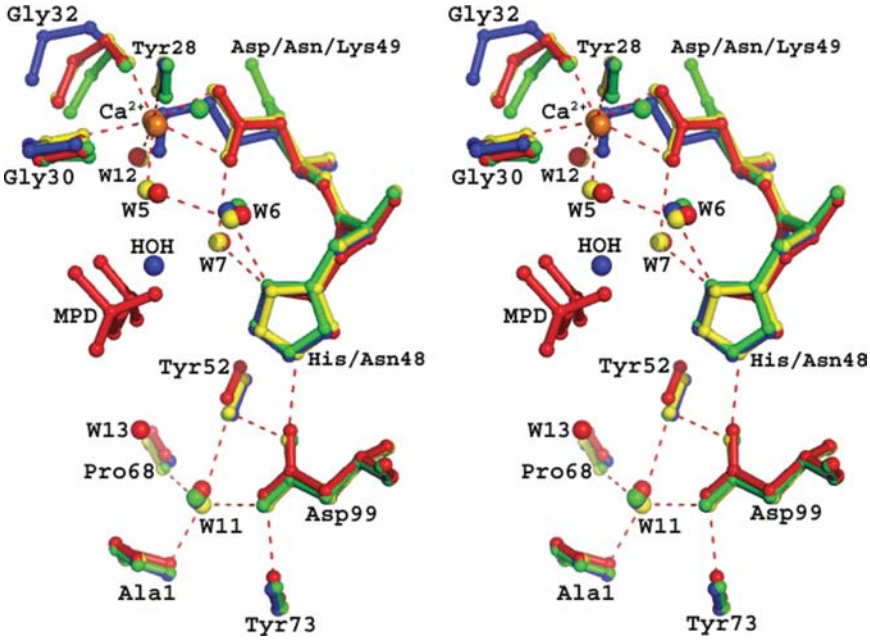

Figure 6
Superposition of the active-site residues and water molecules of the single mutants (H48N, red; D49N, green; D49K, blue) along with the trigonal form of the wild-type enzyme (PDB code 1mkt, yellow).

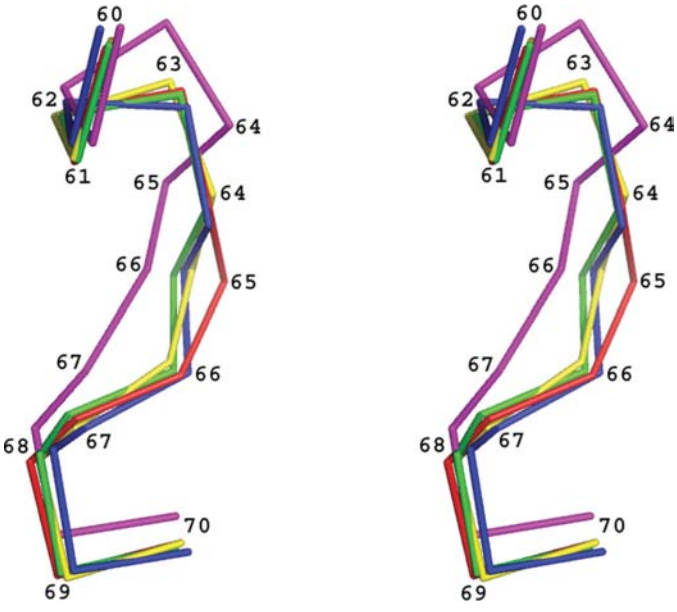

Figure 7
Comparison of the surface-loop region in the three active-site mutants (H48N, red; D49N, green; D49K, blue) with the orthorhombic (PDB code 1une, magenta) and trigonal (PDB code 1mkt, yellow) forms of the wild type.

$N^{\delta2}$ hydrogen bonded to Asp99 $O^{\delta1}$), a molecular-dynamics simulation was also carried out for the alternative orientation. The amide group was found to be flipped to the chosen orientation after 2.76 ns of simulations.

3.2. D49N mutant

The main-chain atoms superpose well with the trigonal form of the wild-type PLA_2, with an r.m.s.d. of 0.3 Å. The functionally important calcium ion is absent, possibly owing to the loss of the negative charge of the mutated residue asparagine, which reduces the affinity of the enzyme for calcium (Fig. 3). However, the catalytic framework along with an extra water molecule (W13) is intact. A Tris molecule is observed and its O atoms are hydrogen bonded to the backbone O atoms of Phe106, Ser107 and Val109. Furthermore, an MPD molecule is also observed near the active-site mouth as in another structure (PDB code 1vl9; Sekar *et al.*, 2005).

Careful examination of the MD trajectory analysis of the single mutant D49N shows water molecules occupying similar positions to W7 (one of the histidine water molecules), W11 (structural water) and its neighbour W13 in the dynamically equilibrated system as observed in the crystal structure. Subsequently, Asp49 was mutated to Asn (*in silico*) in the wild-type structure (PDB code 1mkt) in order to observe the movement of the calcium ion in the 1mkt_D49N mutant during molecular dynamics. The calcium ion was found to move ∼5 nm away from the active site of the enzyme (Fig. 4), well into the solvent region. Fig. 4 shows the protein–calcium ion interaction energy and the distance between the protein and calcium ion with respect to the time of simulation. For comparison, the protein–calcium ion interaction energy and the distance between the protein and calcium ion for the H48N mutant are also shown. From the graph, it is clear that the interaction energy and the distance between the calcium ion and protein are stable throughout the simulation for the mutant H48N, in contrast to the other single mutant D49N.

3.3. D49K mutant

The overall tertiary structure of the D49K mutant is similar to that of the wild type, with an r.m.s.d. of 0.4 Å (backbone atoms only). Superposition of the backbone atoms of the protein ligands (Tyr28, Gly30, Gly32 and Lys49) with the wild-type structure shows a greater change, with an r.m.s.d. of 0.6 Å. The large deviation is a consequence of the longer side chain of the mutated residue lysine. The calcium ion and three water molecules (W5, W7 and W12) are found to be missing. Only the catalytic water molecule W6 is present; it is hydrogen bonded to His48 $N^{\delta1}$. In fact, the atom N^{ζ} occupies the position of the calcium ion. Furthermore, N^{ζ} is hydrogen bonded to the carbonyl O atoms of Tyr28 and Gly30 and the catalytic water W6 (Fig. 5). However, the catalytic framework comprising Ala1, Tyr52, Pro68, Asp99 and the structural water W11 is preserved. Although the active-site calcium ion is not present in the crystal structure of D49K, it was retained in the *in silico* 1mkt_D49K mutant essentially to observe the effect of the mutated residue lysine on the calcium during molecular

dynamics. The mutated residue lysine was modelled using the program *Coot* in such a way that there is no short contact with any other atoms including the active-site calcium ion. The MD calculations of the *in silico* 1mkt_D49K mutant shows that the interaction energy of the calcium ion with protein decreases with simulation time. Therefore, the calcium ion is considered to have moved away from the active site. Interestingly, as observed in the crystal structure, the MD averaged structure of 1mkt_D49K shows that the N^{ζ} atom of the mutated residue lysine occupies a similar position to the calcium ion.

3.4. Active site and surface loop in all three mutants

The active site of the H48N mutant is not disturbed because the calcium ion is tightly bound in the active site. However, in both Asp49 mutants the active site is perturbed owing to the absence of the calcium ion and in turn its coordinating water molecules. In the Asp49 mutants, two calcium-coordinating residues Gly30 and Gly32 have moved away from the active site (Fig. 6) because of the absence of the calcium ion. Furthermore, the movement of Gly32 in the case of the D49K mutant may be a consequence of the longer side chain of Lys49. As expected, the axial and equatorial calcium-coordination water molecules (W12 and W5) are missing from the Asp49 mutants. It is noteworthy that the equatorial calcium-coordination water molecule (W5) is involved in hydrogen bonding (Fig. 1) to the backbone N atom of Gly30 (Sekar & Sundaralingam, 1999). Thus, the functionally important calcium ion is also essential for the integrity of the active site. The electron density for the 11 surface-loop residues (60–70) in all three mutants is not clear at the 1.0σ level. However, the surface loop is modelled at a low contour (0.4σ) level in all three mutants. Fig. 7 shows a comparison of the surface loop of all three mutants and two forms (orthorhombic and trigonal) of the wild-type structure. Most of the crystal structures of bovine pancreatic PLA_2 determined to date indicate that the surface loop is ordered either in the presence of inhibitors or in the presence of a second calcium ion or both, with the exception of two structures (PDB codes 1une and 1g4i; Sekar & Sundaralingam, 1999; Steiner *et al.*, 2001). It is generally observed that the number of water molecules near the surface-loop residues is greater in the case of ordered structures.

The fluctuation of the C^{α} atom of each residue (Fig. 8) throughout the MD simulation reveals that the calcium-binding loop (Gly30 and Gly32) is highly flexible in addition to the surface-loop region in all three mutants. However, in the Asp49 mutants the large fluctuation of Gly30 and Gly32 is primarily because of the mutation at residue 49 and the loss of the calcium ion in the active site. Fig. 8 clearly shows the large movement of residues Gly30 and Gly32 in the D49N (green) and D49K (blue) mutants. Further, in the MD average structures water molecules occupied the void created by these two residues.

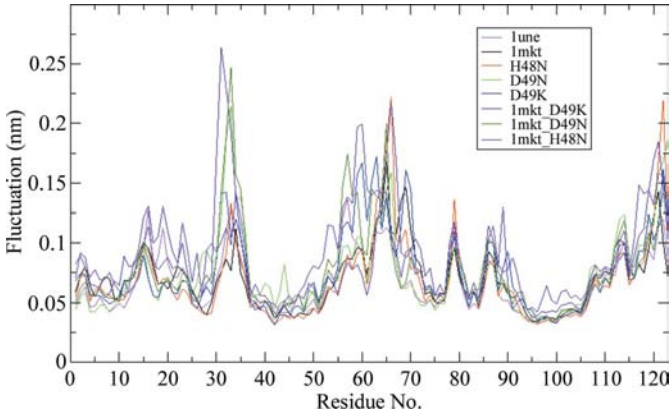

Figure 8
The graph depicts the average fluctuation of all 123 C^{α} atoms using 1500 structures computed every 2 ps. The molecular-dynamics simulation was performed for 3 ns.

3.5. Invariant water molecules

The numbers of water molecules located in the H48N, D49N and D49K mutant crystal structures are 132, 139 and 127, respectively. Approximately 85% of the water molecules are found in the first hydration shell in all three mutants (Shanthi *et al.*, 2003). A careful examination of the water structure in all three mutants reveals that a total of 41 water molecules (including the structural water W11 and the catalytic water W6) are invariant, with average *B* factors of 29.47, 23.82 and 31.18 $Å^2$ for the H48N, D49N and D49K mutants, respectively. Invariant water molecules are identified upon the superposition of the H48N and D49K structures on the structure of D49N to be those which lie within 0.5 Å of the equivalent water molecules in the fixed structure. Since the number of water molecules is greater in the D49N mutant, it was used as a fixed molecule. The structural water molecule (W11) and the catalytic water molecule (W6) are present in all three mutants (Fig. 9). Furthermore, all 41 invariant crystallographic water molecules are present in the

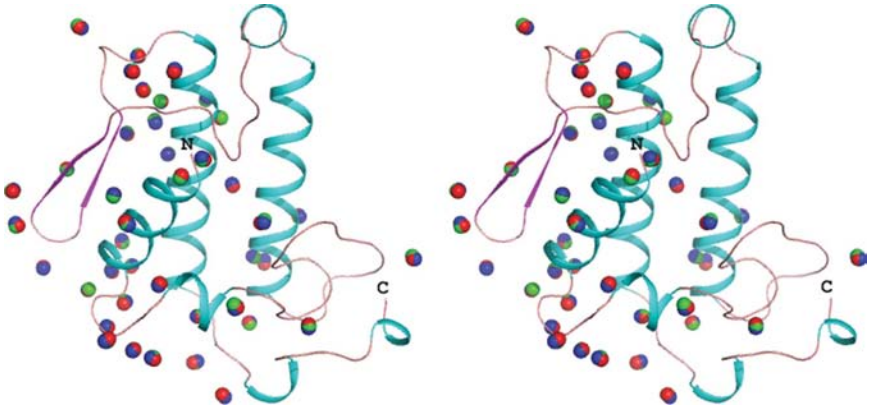

Figure 9
Invariant water molecules of H48N, D49N and D49K mutants shown in red, green and blue colours, respectively. The protein molecule shown here corresponds to the H48N mutant.

corresponding MD average structure computed between 2 and 3 ns. These invariant water molecules form 127, 136 and 128 hydrogen bonds in the H48N, D49N and D49K mutants, respectively. Similar analysis with the MD average structures reveals 192, 198 and 193 interactions, respectively. Interestingly, the hydrogen-bonding interactions of the invariant water molecules are also found in the MD average structure. An increased number of hydrogen bonds in the MD simulated structures are found since they contain more water molecules (643, 638 and 664 in H48N, D49N and D49K, respectively). A total of nine water molecules (excluding W6 and W11) are found in the core of the enzyme. Interestingly, these nine buried water molecules were observed in almost all crystal structures of bovine and porcine pancreatic PLA_2s, indicating possible involvement in the folding of the enzyme. The remaining 30 invariant water molecules are on the surface of the enzyme and are likely to be involved in providing stability to the enzyme by hydrating surface polar residues.

4. Conclusions

The overall tertiary structure of all three mutants is similar to that of the wild-type enzyme. However, the active site is disturbed in the case of the Asp49 mutants and is intact in the H48N mutant. Thus, the crystal structures and molecular-dynamics simulations of the three single mutants confirm that residue Asp49 is important for both calcium binding and the integrity of the active site. On the other hand, His48 is not crucial to the stability of the active site. However, it is important for the catalytic activity of the enzyme. It is clear that the active-site framework remains intact in all the mutant structures and this is further verified by the molecular dynamics. Furthermore, it is interesting to note that the structural water W11 is retained in its position after molecular dynamics; this suggests the importance of this water molecule in maintaining the framework intact. Approximately, 20% of the crystallographic water molecules are conserved in all the three mutants. In addition, water molecules occupy similar positions in the average structures obtained from molecular dynamics.

The intensity data were collected at the National Data Collection Facility for Structural Biology at the Molecular Biophysics Unit, Indian Institute of Science, Bangalore 560 012, India, supported by the Department of Science and Technology (DST) and the Department of Biotechnology (DBT), Government of India. The authors gratefully acknowledge the use of the Interactive Graphics-Based Molecular Modelling (IGBMM), the Supercomputer Education and Research Centre (SERC) and the Distributed Information Centre. One of the authors (KS) thanks the DST for financial support.

References

Berg, B. van den, Tessari, M., Boelens, R., Dijkman, R., de Haas, G. H., Kaptein, R. & Verheij, H. M. (1995). *Nature Struct. Biol.* **2**, 402–406.
Bergh, C. J. van den, Slotboom, A. J., Verheij, H. M. & de Haas, G. H. (1988). *Eur. J. Biochem.* **176**, 353–357.
Brünger, A. T. (1992). *Nature (London)*, **355**, 472–475.
Brünger, A. T., Adams, P. D., Clore, G. M., DeLano, W. L., Gros, P., Grosse-Kunstleve, R. W., Jiang, J.-S., Kuszewski, J., Nilges, M., Pannu, N. S., Read, R. J., Rice, L. M., Simonson, T. & Warren, G. L. (1998). *Acta Cryst.* D**54**, 905–921.
Collaborative Computational Project, Number 4 (1994). *Acta Cryst.* D**50**, 760–763.
Darden, T. D. & York, P. L. (1993). *J. Chem. Phys.* **98**, 10089–10092.
Davidson, F. F. & Dennis, E. A. (1990). *J. Mol. Evol.* **31**, 228–238.
Davis, I. W., Murray, L. W., Richardson, J. S. & Richardson, D. C. (2004). *Nucleic Acids Res.* **32**, W615–W619.
Deenen, L. L. van & de Hass, G. H. (1964). *Adv. Lipid. Res.* **2**, 167–234.
Dijkstra, B. W., Drenth, J., Kalk, K. H. & Vandermaelen, P. J. (1978). *J. Mol. Biol.* **124**, 53–60.
Dijkstra, B. W., Kalk, K. H., Hol, W. G. & Drenth, J. (1981). *J. Mol. Biol.* **147**, 97–123.
Dupureur, C. M., Yu, B. Z., Jain, M. K., Noel, J. P., Deng, T., Li, Y., Byeon, I. J. & Tsai, M. D. (1992). *Biochemistry*, **31**, 6402–6413.
Dupureur, C. M., Yu, B. Z., Mamone, J. A., Jain, M. K. & Tsai, M. D. (1992). *Biochemistry*, **31**, 10576–10583.
Emsley, P. & Cowtan, K. (2004). *Acta Cryst.* D**60**, 2126–2132.
Hess, B., Bekker, H., Berendsen, H. J. C. & Fraaije, J. G. E. M. (1997). *J. Comput. Chem.* **18**, 1463–1472.
Hussain, A. S. Z., Shanthi, V., Sheik, S. S., Jeyakanthan, J., Selvarani, P. & Sekar, K. (2002). *Acta Cryst.* D**58**, 1385–1386.
Jorgensen, W. L., Maxwell, D. S. & Tirado-Rives, J. (1996). *J. Am. Chem. Soc.* **118**, 11225–11236.
Kaminski, G. A., Friesner, R. A., Tirado-Rives, J. & Jorgensen, W. L. (2001). *J. Phys. Chem. B*, **105**, 6474–6487.
Laskowski, R. A., MacArthur, M. W., Moss, D. S. & Thornton, J. M. (1993). *J. Appl. Cryst.* **26**, 283–291.
Leatherbarrow, R. J. & Fersht, A. R. (1987). *Biochemistry*, **26**, 8524–8528.
Li, Y. & Tsai, M. D. (1993). *J. Am. Chem. Soc.* **115**, 8523–8526.
Li, Y., Yu, B. Z., Zhu, H., Jain, M. K. & Tsai, M. D. (1994). *Biochemistry*, **33**, 14714–14722.
McCoy, A. J., Grosse-Kunstleve, R. W., Adams, P. D., Winn, M. D., Storoni, L. C. & Read, R. J. (2007). *J. Appl. Cryst.* **40**, 658–674.
McDonald, I. K. & Thornton, J. M. (1994). *J. Mol. Biol.* **238**, 777–793.
Noel, J. P., Bingman, C. A., Deng, T. L., Dupureur, C. M., Hamilton, K. J., Jiang, R. T., Kwak, J. G., Sekharudu, C., Sundaralingam, M. & Tsai, M. D. (1991). *Biochemistry*, **30**, 11801–11811.
Otwinowski, Z. & Minor, W. (1997). *Methods Enzymol.* **276**, 307–326.
Read, R. J. (2001). *Acta Cryst.* D**57**, 1373–1382.
Schüttelkopf, A. W. & van Aalten, D. M. F. (2004). *Acta Cryst.* D**60**, 1355–1363.
Sekar, K. (2007). *Curr. Topics Med. Chem.* **7**, 779–785.
Sekar, K., Biswas, R., Li, Y., Tsai, M.-D. & Sundaralingam, M. (1999). *Acta Cryst.* D**55**, 443–447.
Sekar, K., Gayathri, D., Velmurugan, D., Jeyakanthan, J., Yamane, T., Poi, M.-J. & Tsai, M.-D. (2006). *Acta Cryst.* D**62**, 392–397.
Sekar, K., Rajakannan, V., Gayathri, D., Velmurugan, D., Poi, M.-J., Dauter, M., Dauter, Z. & Tsai, M.-D. (2005). *Acta Cryst.* F**61**, 3–7.
Sekar, K., Sekharudu, C., Tsai, M. D. & Sundaralingam, M. (1998). *Acta Cryst.* D**54**, 342–346.
Sekar, K. & Sundaralingam, M. (1999). *Acta Cryst.* D**55**, 46–50.
Shanthi, V., Rajesh, C. K., Jayalakshmi, J., Vijay, V. G. & Sekar, K. (2003). *J. Appl. Cryst.* **36**, 167–168.
Spoel, D. van der, Lindahl, E., Hess, B., Groenhof, G., Mark, A. E. & Berendsen, H. J. C. (2005). *J. Comput. Chem.* **26**, 1701–1718.

Steiner, R. A., Rozeboom, H. J., de Vries, A., Kalk, K. H., Murshudov, G. N., Wilson, K. S. & Dijkstra, B. W. (2001). *Acta Cryst.* D**57**, 516–526.
Sumathi, K., Ananthalakshmi, P., Roshan, M. N. A. & Sekar, K. (2006). *Nucleic Acids Res.* **34**, W128–W138.
Verheij, H. M., Slotboom, A. J. & de Haas, G. H. (1981). *Rev. Physiol. Biochem. Pharmacol.* **91**, 91–203.
Verheij, H. M., Volwerk, J. J., Jansen, E. H., Puyk, W. C., Dijkstra, B. W., Drenth, J. & de Haas, G. H. (1980). *Biochemistry*, **19**, 743–750.